Mathematical multi-physics modeling and simulation of a solid oxide fuel cell unit for thermo-mechanical stress analyses

Konrad W. Eichhorn Colombo[1,*], Vladislav V. Kharton[2], Filippo Berto[3], Nicola Paltrinieri[3]

[1]*Department of Chemical Engineering, Norwegian University of Science and Technology (NTNU), Trondheim, Norway*

[2]*Institute of Solid State Physics RAS, Moscow District, Chernogolovka, Russian Federation*

[3]*Department of Mechanical and Industrial Engineering, NTNU, Trondheim*

Abstract: We use a mathematical model of a solid oxide fuel cell (SOFC) unit for stress analyses. The model comprises a thermo-electrochemical-chemical performance model that calculates the temperature field in the solid part which is then used as input for the thermo-mechanical stress model. The level of detail allow system analyses with computational efficiency. Displacement is used as primary variable for stress calculations and thermo-mechanical failure probabilities. The operation envelope of the SOFC unit is defined through design and operational constraints. The applied multi-physics approach combines the disciplines of process design, material science as well as control engineering, and also emphasises the importance of using advanced mathematical modeling and simulation techniques to address problems of practical relevance.

*E-mail: konrad.eichhorn@ntnu.no.

List of symbols

A	area [m^2]
a	activity [-], constant for degradation rate [-]
C	gas concentration [mol/m^3]
c_p	heat capacity [J/(mol K)]
E	Young's modulus [Pa]
E°	Gibbs potential [V]
F	Faraday constant [C/mol]
FU	fuel utilization [-]
Δh	enthalpy change of reaction [J/mol]
h_c	heat transfer coefficient [$W/(m^2\ K)$]
i	current density [A/m^2]
I	current [A]
L	length [m]
M	number of cell bundles [-]
m	Weibull modulus [-]
$\dot{m}$	mass flow [kg/s]
N	number of stacks [-]
$\dot{n}$	mole flow [mol/s]
p	partial pressure [Pa]
P	power [W]
P_f	failure probability [-]
R	universal gas constant [J/(mol K)], ohmic resistance [Ω]
r	radius, spatial distribution variable in radial direction [m]
$\dot{r}$	reaction rate [mol/s]
t	time [s, hr]
u	displacement [m]
v	fluid velocity [m/s]
V	voltage [V]
T	temperature [K]
$\tilde{T}$	temperature difference between operation temperature and sintering temperature [K]
T^o	reference/sintering temperature [K]
z	number of electrons exchanged in global reaction [-], spatial distribution variable in axial direction [m]
α	thermal expansion coefficient [1/K]
β	constant for Butler-Volmer equation [-]
γ	constant for activation polarisation [A/m^2]
λ	thermal conductivity [W/(K m)], first Lamé coefficient [-]
η	overpotential [-], efficiency [-]
ρ	density [kg/m^3]
ε	strain [Pa]
μ	second Lamé coefficient [-]
ν	Poisson ratio [-]
σ	stress [Pa]
σ_o	characteristic strength [Pa]
τ	shear stress [Pa]
[..]	closed interval for boundary condition
(..)	open interval for boundary condition

List of subscripts

act	activation polarisation loss
con	concentration polarisation loss
g	gaseous
i	chemial specie
ohm	ohmic loss
r	spatial r-direction
s	solid material
z	spatial z-direction
θ	spatial θ-direction

List of superscripts

an	anode
ca	cathode
el	electrolyte

1 Introduction

Fuel cell systems continue to receive much attention because of their potential as an important building block for sustainable energy solutions [1, 2, 3, 4, 5, 6, 7, 8, 9]. The most promising fuel cell types for application in micro-(combined heat and power) systems are solid oxide fuel cell (SOFC) and proton exchange membrane fuel cell technologies. Due to high operating temperatures, SOFCs can employ non-precious metal, earth-abundant oxide electro-catalysts, or both. Furthermore, in SOFC systems gaseous and liquid hydrocarbons as well as solid fuels can be utilized and converted into electricity. Operation of SOFCs in reverse mode offers, in principle, the opportunity to produce fuels at low power demand, which can afterwards be consumed again by the system. However, such switching may be problematic from a durability point of view [10, 11, 12], also leading to additional requirements in terms of functional properties and stability of the electrodes' materials. In fact, for a wide commercialization the system's lifetime needs to be further improved.

Analysis of fuel cell stacks have been studied relatively extensively from primarily two perspectives. First, from a thermodynamic perspective where the mathematical formulation ranges from lumped steady state to spatially distributed dynamic models. Second, from a materials and mechanical perspective, with a strong focus on finding material combinations which lead to high performance and proper combined stability. The need to merge these two perspectives has already been identified some time ago because the thermodynamic and kinetic phenomena are strongly linked to mechanical properties and vice versa.

Refs. [13, 14, 15, 16, 17, 18, 19, 20] present analyses from a systems perspective for SOFCs. Ref. [21] presents a review of thermo-mechanical modeling of SOFCs. Other electrochemical systems were also analysed with this modeling approach (see e.g., Refs. [22, 23, 24, 25]). At the heart of this multi-physics modeling and simulation approach is the physical description by means of partial differential equations. The purely data-driven approach is not further discussed here as we regard it as an auxiliary element rather than an alternative.

The main general purpose of this paper is to present the thermo-mechanical extension of the performance model adopted from Refs. [26, 27]. The temperature field for the electrolyte

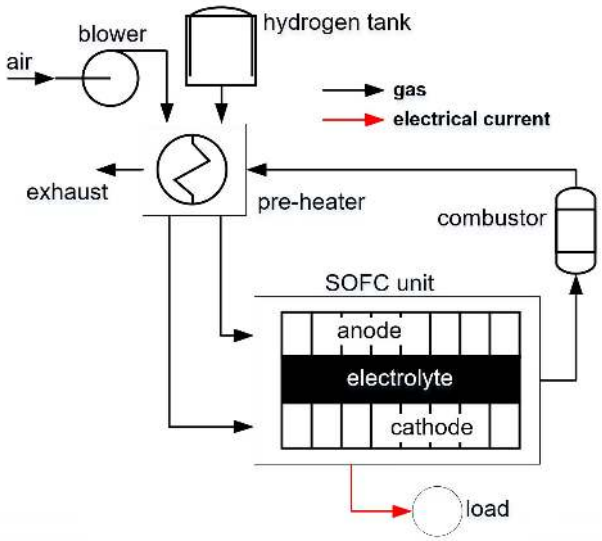

Figure 1: Solid oxide fuel cell (SOFC) system.

and electrodes is fed to a thermo-mechanical stress model. The thermo-mechanical stress model was validated against that from Ref. [14] and showed good agreement.

2 Solid oxide fuel cell unit

Figure 1 shows a simple SOFC-based system with hydrogen as fuel. This configuration is one of the simplest possible for fuel cells operating at elevated temperatures. In this work the focus is on the SOFC stack, but input data are obtained from simulations of this system.

2.1 Principal operation

A simplified fuel cell scheme comprises five components, i.e. two gas channels and three ceramic or composite layers. Its operation requires also two metallic current collectors (interconnects) and a sealant. The gas channels provide the fluid for reduction (cathode) and oxidation (anode), respectively. Between anode and cathode there is an oxygen-ion conducting solid electrolyte. Charge neutrality and movement of negative charges (electrons) is provided through an outer electrical circuit. The principal mechanism in an individual SOFC is shown in Figure 2.

In the electrochemical cell, oxygen ions are transported from the cathode across the electrolyte membrane to the anode according to the following half-cell reactions on the cathode (oxygen reduction) and the anode (fuel oxidation), respectively [28]

$$\begin{aligned} O_2 + 4e^- &\rightleftharpoons 2O^{2-} \\ 2H_2 + 2O^{2-} &\rightleftharpoons 2H_2O + 4e^- \end{aligned} \tag{1}$$

with the resulting global equilibrium reaction

$$2H_2 + O_2 \rightleftharpoons 2H_2O \tag{2}$$

In this work, a tubular design of the SOFC unit is assumed [29, 30, 31, 32], shown in Figure 3.

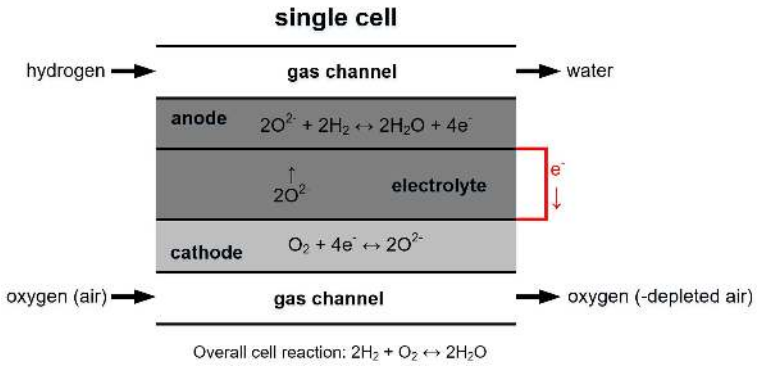

Figure 2: Principle of a solid oxide fuel cell (SOFC) with hydrogen as fuel.

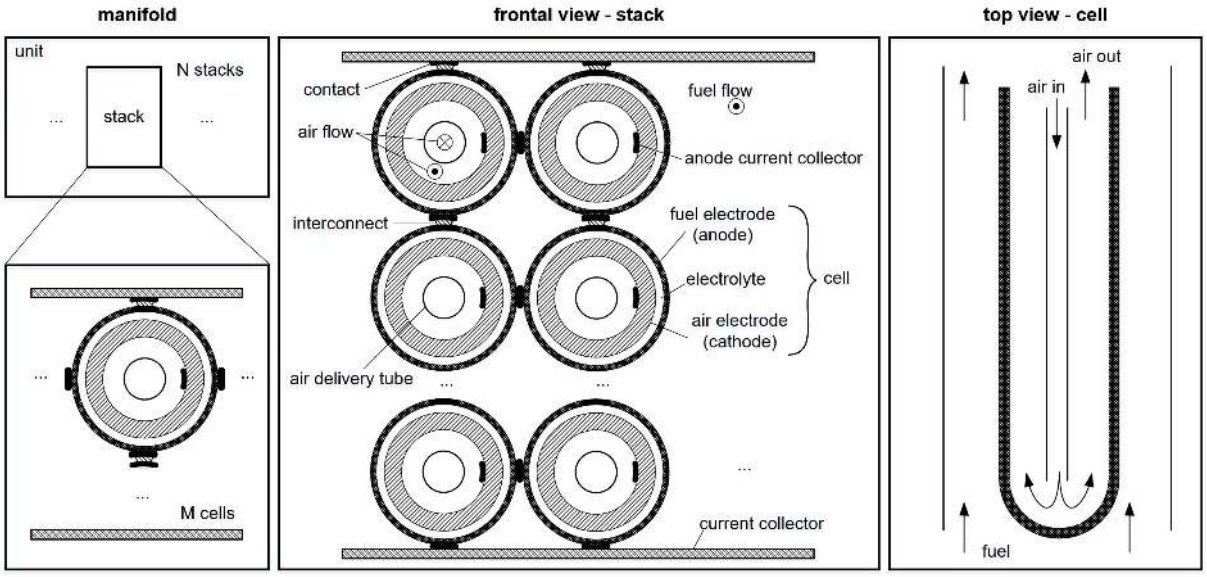

Figure 3: SOFC unit with part of the repeating manifold of the tubulur solid oxide fuel stacks and cells design.

Table 1: Design and operation constraints.

constraint	**potential effect**	**limit**
max. leakage rate (interconnects)	performance loss, failure due to leakage	0.1%
power density	concentration polarization, cell degradation	80-90% of max.
max. impurities concentration	performance loss, degradation, failure	30%
max. difference in thermal expansion coefficients	performance loss and failure due to thermo-mechanical stresses	10-17%
temperature gradients (transient)	performance loss, failure due to thermo-mechanical stresses	20K/cm
max. temperature differences along stack	performance loss, failure due to thermo-mechanical stresses	150K
max. temperature	performance loss, failure due to thermo-mechanical stresses and chemical interaction	1300K
min. temperature	performance loss, failure due to thermo-mechanical stresses	900K
max. fuel utilization	fuel starvation, efficiency loss	90%
min. fuel utilization	thermo-mechanical stresses	40%
max. total pressure difference between fluid streams	mechanical stress	3bar

2.2 Design and operation constraints

SOFC stacks are complex systems in which thermal, electrochemical, chemical, and mechanical phenomena are strongly interlinked. The values of several physical properties are thus dependent on state conditions. The operation envelope of the SOFC unit is constrained by hard or soft constraints. Operation beyond hard constraints is not possible. While soft constraints can, but should not be exceeded, e.g. to avoid loss of performance, high failure probabilities, or both. Table 1 lists some critical design and operation constraints. Further constraints will need to be considered for balance-of-plant system components (not further discussed in this paper).

3 Mathematical model

In this section the mathematical model is briefly presented. The connection between the thermo-electrochemical-chemical and thermo-mechanical sub-models is shown in Figure 4. The mathematical model was implemented in gPROMS [33], which solves complex large-scale problems of index one. The model consists of about 18k algebraic and 1k differential equations.

3.1 Model assumptions

General assumptions for the mathematical model are as follows:

- pure hydrogen as fuel
- steady state conditions

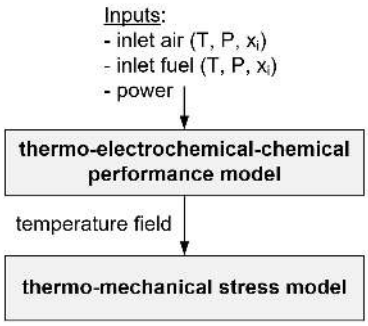

Figure 4: Link between the thermo-electrochemical-chemical performance model and thermo-mechanical stress model.

- effects due to current collectors and sealants are neglected
- symmetry in circumferential θ-direction
- bundle effects in stack are neglected [26, 27]
- electrical potential reduction due to activation polarisation and concentration polarisation as well ohmic losses [26, 27]
- heat transport between gas and solid based on Newton's law [26, 27]
- heat transport in solid due to conduction [26, 27]
- heat generation in solid due to electrochemical reaction is accounted for [26, 27]
- one-dimensional discretisation of gas channels (axial), plug flow, laminar flow [26, 27]
- two-dimensional discretisation of solid (axial and radial) [26, 27]
- stress-free conditions at sintering temperature (homogeneously distributed) [34]
- thermo-mechanics are based on Navier equations and Hooke's law [35, 36]
- stresses in the solids occur due to temperature and pressure differences [37]
- boundary conditions defined at interfaces between gas phase and electrodes as well as between electrolyte and electrodes
- mechanically supported at cathode (one end), i.e. displacement defined; all other ends of solid materials are free [14] (Figure 5)
- dependencies (e.g., on temperature) for thermodynamic [26, 27] and thermo-mechanical properties (Table 2 and associated equations) are included
- Weibull approach for failure probability due to thermo-mechanical stresses [38, 39]

3.2 Energy conservation

Heat transfer between the gases and solid is given by [26, 27]

$$v_g \frac{\partial T_g c_{p,g} \rho_g}{\partial z} = \frac{2 h_c}{r} (T_s - T_g). \tag{3}$$

The spatially distributed energy balance in axial and radial direction for the solids is [26, 27]

$$0 = \lambda_s \nabla^2 T_s, \tag{4}$$

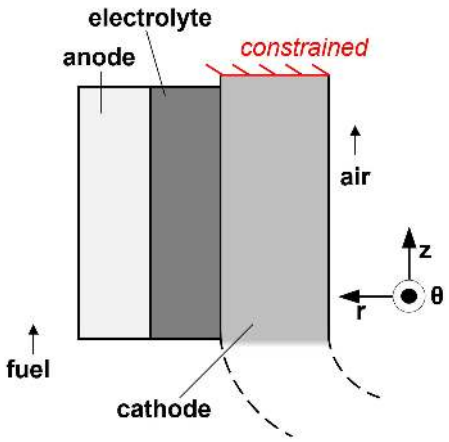

Figure 5: Geometry of the tubular SOFC with the individual layers.

with the following boudary condition between fuel and the anode, including heat generation through the electrochemical reaction [26, 27]

$$\lambda_s \frac{\partial T_s}{\partial r} = h_c(T_s - T_g) + \frac{\dot{r}\Delta h}{2\pi r L}, \tag{5}$$

where the reaction rate follows [26, 27]

$$\dot{r} = \frac{iA}{2F}. \tag{6}$$

3.3 Mass conservation

Mass conservation for the gases follows [26, 27]

$$v_g \frac{\partial C_i}{\partial z} = \dot{r} \tag{7}$$

3.4 Momentum conservation

Spatial distribution in momentum were neglected. But pressure drops in both gas streams were considered using Reynolds number and friction factor correlations (laminar flow) [40, 26]

$$f = \frac{64}{Re} \tag{8}$$

3.5 Electrochemistry

The cell voltage is [28]

$$V_{cell} = V_{OC} - \eta_{act}^{an} - \eta_{act}^{ca} - \eta_{con}^{an} - \eta_{con}^{ca} - \eta_{ohm}. \tag{9}$$

The open circuit voltage (OCV) is given by the Nernst equation [28]

$$V_{OC} = E^{\circ} + \frac{RT}{zF} ln \frac{a_{oxi}}{a_{red}}. \tag{10}$$

The activation polarization losses on anode and cathode are given implicitly by the Butler-Volmer equation [28]

$$i_i = i_i^{\circ} \left[exp\left(\frac{n_i \beta_{fi} F \eta_{act,i}}{RT} \right) - exp\left(- \frac{n_i \beta_{ri} F \eta_{act,i}}{RT} \right) \right]. \tag{11}$$

The concentration polarization losses describe interactions between the bulk gas phase to electrode surfaces as well as between electrode surfaces and triple-phase boundary (TPB)

$$\eta_{con,i} = \frac{RT}{n_i F} ln(p_{i,g}, p_{i,TPB}). \tag{12}$$

The ohmic loss is

$$\eta_{ohm} = iAR, \tag{13}$$

with an ohmic resistance comprising temperature-dependent layer resistivity of electrodes and electrolyte and a constant resistivity for the interconnects [26, 27].

3.6 Thermo-mechanics

The displacement is used as the primary unknown variable. Deformations and displacements of solid are relatively small resulting in a system of linear equations [41]. The Navier equations for the three solid materials in cylindrical coordinates are [35, 36]

$$\begin{aligned} \mu\left(\nabla^2 u_r - \frac{u_r}{r^2}\right) + (\lambda+\mu)\frac{\partial}{\partial r}\left(\frac{1}{r}\frac{\partial}{\partial r}(ru_r) + \frac{\partial u_z}{\partial z}\right) &= \beta\frac{\partial \tilde{T}}{\partial r}, \\ \mu\nabla^2 u_z + (\lambda+\mu)\frac{\partial}{\partial z}\left(\frac{1}{r}\frac{\partial}{\partial r}(ru_r) + \frac{\partial u_z}{\partial z}\right) &= \beta\frac{\partial \tilde{T}}{\partial z}. \end{aligned} \tag{14}$$

The displacements for the three solid materials are related to the strains according to [36]

$$\begin{aligned} \varepsilon_r &= \frac{\partial u_r}{\partial r}, \\ \varepsilon_\theta &= \frac{u_r}{r}, \\ \varepsilon_z &= \frac{\partial u_z}{\partial z}, \\ \varepsilon_{zr} = \varepsilon_{rz} &= \frac{1}{2}\left(\frac{\partial u_r}{\partial z} + \frac{\partial u_z}{\partial r}\right). \end{aligned} \tag{15}$$

The stress-strain relations for the three solid materials are given by Hooke's law [36]

$$\begin{aligned} \sigma_i = \lambda(\varepsilon_r + \varepsilon_\theta + \varepsilon_z) + 2\mu\varepsilon_i - \beta\tilde{T} \text{ , with } i = r, \theta, z, \\ \tau_{zr} = \tau_{rz} = 2\mu\varepsilon_{zr}. \end{aligned} \tag{16}$$

The following subsections show the boundary conditions for the three materials (electrodes, electrolyte) as part of the thermo-mechanical stress model. The direction of representation is from the inner to the outer radius, i.e. from the air channel to the solid material (cathode, electrolyte, anode) and then to the fuel channel. As mentioned earlier, the solid material is fixed at one end of the cathode (cathode-supported) whilst all other ends are free [14] (Figure 5). For an effective and lean representation, boundary conditions for the bulk material do not show the respective material index (e.g., '*ca*'). Notice the difference between open and closed intervals.

Interface between cathode and air channel

The following boundary conditions are valid for $r = r_{in}^{ca}$ and $\forall z \in [0, L]$ [35, 36, 37]

$$2\mu\frac{\partial u_r}{\partial r} + \lambda\varepsilon - \beta\tilde{T} - P_{air} = 0 \tag{17}$$

$$\mu\left(\frac{\partial u_r}{\partial z} + \frac{\partial u_z}{\partial r}\right) = 0 \tag{18}$$

Cathode bulk material

The following boundary conditions are valid $\forall r \in (r_{in}^{ca}, r_{out}^{ca})$ [35, 36, 37]

$$u_z = 0 \ , \quad z = 0, \tag{19}$$

$$2\mu \frac{\partial u_z}{\partial z} + \lambda\varepsilon - \beta\tilde{T} = 0 \ , \quad z = L, \tag{20}$$

$$\mu\left(\frac{\partial u_r}{\partial z} + \frac{\partial u_z}{\partial r}\right) = 0 \ , \quad z = L. \tag{21}$$

Notice here that the Navier equation for the calculation of radial displacement u_r is continued for $z = 0$ (see difference to the set of boundary conditions for electrolyte and anode).

Interface between cathode and electrolyte

The following boundary conditions are valid for $r_{in}^{el} = r_{out}^{ca}$ and $\forall z \in [0, L]$ [35, 36, 37]

$$u_r^{el} = u_r^{ca}, \tag{22}$$

$$u_z^{el} = u_z^{ca}, \tag{23}$$

$$2\mu \frac{\partial u_r^{el}}{\partial r} + \lambda\varepsilon^{el} - \beta\tilde{T}^{el} = 2\mu \frac{\partial u_r^{ca}}{\partial r} + \lambda\varepsilon^{ca} - \beta\tilde{T}^{ca}, \tag{24}$$

$$\mu\left(\frac{\partial u_r^{el}}{\partial z} + \frac{\partial u_z^{el}}{\partial r}\right) = \mu\left(\frac{\partial u_r^{ca}}{\partial z} + \frac{\partial u_z^{ca}}{\partial r}\right). \tag{25}$$

Electrolyte bulk material

The following boundary conditions are valid $\forall r \in (r_{in}^{el}, r_{out}^{el})$ [35, 36, 37]

$$2\mu \frac{\partial u_z}{\partial z} + \lambda\varepsilon - \beta\tilde{T} - P_{fuel} = 0 \ , \quad z = 0, \tag{26}$$

$$\mu\left(\frac{\partial u_r}{\partial z} + \frac{\partial u_z}{\partial r}\right) = 0 \ , \quad z = 0, \tag{27}$$

$$2\mu \frac{\partial u_z}{\partial z} + \lambda\varepsilon - \beta\tilde{T} - P_{fuel} = 0 \ , \quad z = L, \tag{28}$$

$$\mu\left(\frac{\partial u_r}{\partial z} + \frac{\partial u_z}{\partial r}\right) = 0 \ , \quad z = L. \tag{29}$$

Interface between anode and electrolyte

The following boundary conditions are valid for $r_{in}^{an} = r_{out}^{el}$ and $\forall z \in [0, L]$ [35, 36, 37]

$$2\mu \frac{\partial u_r^{el}}{\partial r} + \lambda\varepsilon^{el} - \beta\tilde{T}^{el} = 2\mu \frac{\partial u_r^{an}}{\partial r} + \lambda\varepsilon^{an} - \beta\tilde{T}^{an}, \tag{30}$$

$$\mu\left(\frac{\partial u_r^{el}}{\partial z} + \frac{\partial u_z^{el}}{\partial r}\right) = \mu\left(\frac{\partial u_r^{an}}{\partial z} + \frac{\partial u_z^{an}}{\partial r}\right), \tag{31}$$

$$u_r^{el} = u_r^{an}, \tag{32}$$

$$u_z^{el} = u_z^{an}. \tag{33}$$

Table 2: Thermo-elastic properties of SOFC component materials.

component	**material**	E **[GPa]**	ν **[-]**	α **[1E-6 K^{-1}]**	σ_o **[MPa]**	m **[-]**
anode (reduced)	Ni-3YSZ	$f_2(T)$ [42]	0,387 [42]	12,6	115,2 [14]	6 [14]
electrolyte	8YSZ	$f_3(T)$ [42]	0,31 [42]	10,9 [42]	52 [14]	6 [14]
cathode	LSM	41 [43]	0,28 [43]	12 [44]	446 [45]	7 [45]

Anode bulk material

The following boundary conditions are valid $\forall r \in (r_{in}^{an}, r_{out}^{an})$ [35, 36, 37]

$$2\mu\frac{\partial u_z}{\partial z} + \lambda\varepsilon - \beta\tilde{T} - P_{fuel} = 0 \ , \quad z = 0, \tag{34}$$

$$\mu\left(\frac{\partial u_r}{\partial z} + \frac{\partial u_z}{\partial r}\right) = 0 \ , \quad z = 0, \tag{35}$$

$$2\mu\frac{\partial u_z}{\partial z} + \lambda\varepsilon - \beta\tilde{T} - P_{fuel} = 0 \ , \quad z = L, \tag{36}$$

$$\mu\left(\frac{\partial u_r}{\partial z} + \frac{\partial u_z}{\partial r}\right) = 0 \ , \quad z = L. \tag{37}$$

Interface between anode and fuel channel

The following boundary conditions are valid for $r = r_{out}^{an}$ and $\forall z \in [0, L]$ [35, 36, 37]

$$2\mu\frac{\partial u_r}{\partial r} + \lambda\varepsilon - \beta\tilde{T} - P_{fuel} = 0, \tag{38}$$

$$\mu\left(\frac{\partial u_r}{\partial z} + \frac{\partial u_z}{\partial r}\right) = 0. \tag{39}$$

The temperature field of the solid is given by

$$\tilde{T}(r, z) = T(r, z) - T^o. \tag{40}$$

The initial stress distribution during the sintering process, and hence the reference temperature, is assumed to be homogeneously distributed in the material. Thermo-mechanical parameters are as follows with the input parameters given in Table 2 [35, 36]

$$\begin{aligned} \lambda(z) &= \frac{E(z)\nu}{(1+\nu)(1-2\nu)}, \\ \mu(z) &= \frac{E(z)}{2(1+\nu)}, \\ \beta(z) &= \frac{\alpha E(z)}{1-2\nu}. \end{aligned} \tag{41}$$

3.7 Failure probability

Solving the eigenvalue problem leads to the following equation system to obtain the principal stresses [39]

$$\begin{aligned} \sigma_r + \sigma_\theta + \sigma_z &= \sigma_1 + \sigma_2 + \sigma_3, \\ \frac{1}{2}((\sigma_r + \sigma_\theta + \sigma_z)^2 - \tau_{rz}^2) &= \sigma_1\sigma_2 + \sigma_2\sigma_3 + \sigma_3\sigma_1, \\ \sigma_r\sigma_\theta\sigma_z - \tau_{rz}^2\sigma_\theta &= \sigma_1\sigma_2\sigma_3. \end{aligned} \tag{42}$$

The calculation of the SOFC stack's overall failure probability for brittle material is then obtained by [38, 39]

$$P_f = 1 - \prod_{j=1}^{3}\prod_{i=1}^{3} exp\left(- \frac{1}{V_{ref}} \int_V \left(\frac{\sigma_i}{\sigma_o}\right)^m dV \right) \; \forall \sigma_i \leq 0 \text{ (0 otherwise)}. \tag{43}$$

Input parameter values for the calculation of the survival and overall failure probabilities are listed in Table 2. The failure probability used in this work is a well-established approach but may have limitations when applied to systems operating under non-laboratory conditions. In this work hydrogen is used as fuel. Fuels containing carbon can lead to carbon deposition on the Ni-YSZ cermet anode and can thus alter the material [46, 47, 48]. Sulphur species in fluids can react with the hydrogen from the fuel or oxygen ions from the cathode-electrolyte which leads to the formation of H_2S and SO_2, respectively [49, 50]. Other chemical species which commonly occur in standard fuels can also have a detrimental effect on the durability of the SOFC system. These effects are disregarded here.

4 Results and discussion

Table 3 shows input parameters, and results for depending variables, for the thermo-electro-chemical-chemical performance model to generate the temperature field for the thermo-mechanical stress model. With the total current density, fuel utilisation and mean solid material temperature as degrees of freedom for simulation, the power output, voltage and fluid mole flows at the inlets are determined[1]. These values were obtained from simulations with the entire system shown in Figure 1, also including the balance-of-plant process components. Figure 6 shows the solid material temperature (average in radial direction) and fluid temperatures as well as the temperature-dependent current density in axial direction of the SOFC stack. The temperature field is input for the thermo-mechanical stress model (see Figure 4). Table 4 shows a comparison between the chosen design conditions and specified constraints. Table 1 shows a comparison of actual operation conditions in the simulation and specified design and operation constraints (Table 1). Also included was the temperature gradient in axial direction, which is of particular interest during transients. All constraints are respected for the chosen operation point.

Figure 7 shows the displacement for the electrolyte and electrodes in axial direction. Comparison of the slopes of the mean solid temperature (Figure 6) with the displacements shows a strong correlation. For the chosen operation conditions displacements in the z-coordinate are higher than in the corresponding r-coordinate. A displacement of material means changes in the physical dimensions. Mismatches in physical properties leading to different displacements of adjacent materials can cause breakage. One possible failure scenario is the mixing of fuel (here hydrogen) and oxidant at elevated temperature, which must be avoided from a safety

[1] Essentially any variable in the model can act as input parameter as long as the model remains well-posed.

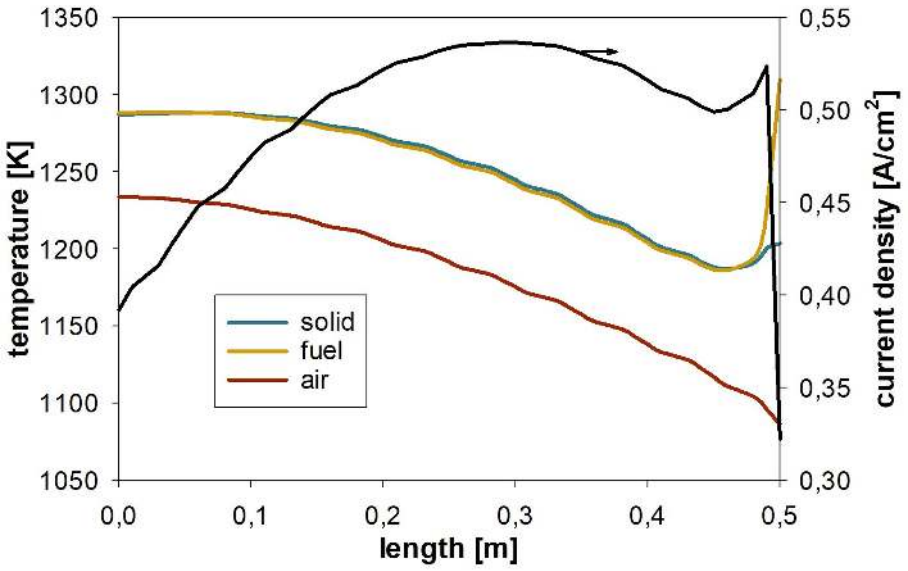

Figure 6: Temperature and current density distribution over stack length.

perspective. Figure 8, Figure 9 and Figure 10 show the spatial distribution of stresses in the electrolyte, cathode and anode, respectively. Material boundaries are mathematical singularities which can lead to physical excessive stresses or stress variations in their distribution, or both. The strong temperature-dependency is again visible. Table 5 shows the resulting survival probabilities for the electrolyte and anodes as well as overall failure probability. The operation conditions led to relatively high survival probabilities and a low failure probability. Failure on a cell level (see Figure 3) can propagate further to the stack and unit level. In this work, all cells are considered as equal.

Figure 11 shows results from a sensitivity analysis with respect to the ratio between the air and fuel channel pressure, and the mean solid temperature whilst all other input parameters were kept constant. The failure probability decreased with increasing pressure ratio. The failure probability decreases with increasing pressure ratio. In Table 1, however, a maximum pressure difference of three bar was specified. Exceeding this value makes mechanical failure more likely. Increasing the mean solid temperature, i.e. the mean operation temperature of the unit, reduces the calculated failure probability because the difference between this and the sintering temperature gets smaller and thus also the force term in the Navier equations. The obtained overall failure probabilities for these cases were relatively high. It is emphasised that operation conditions, in particular those leading in larger differences between the temperature field and initial stress temperature will generate larger stresses and therefore also to higher failure probabilities.

5 Conclusion

A mathematical model of an SOFC unit was simulated for stress analyses and overall failure probabilities by means of the Weibull approach. Operation conditions (steady state) were obtained from simulations on a system level which also comprised balance-of-plant process components. The cases presented here show all relatively low failure probabilities (<3%). However, simulations also revealed a strong thermo-mechanical coupling and therefore dependency of stress distribution on the actual operation conditions. Any changes that increase the force term, e.g. temperature differences between the actual operation and reference tem-

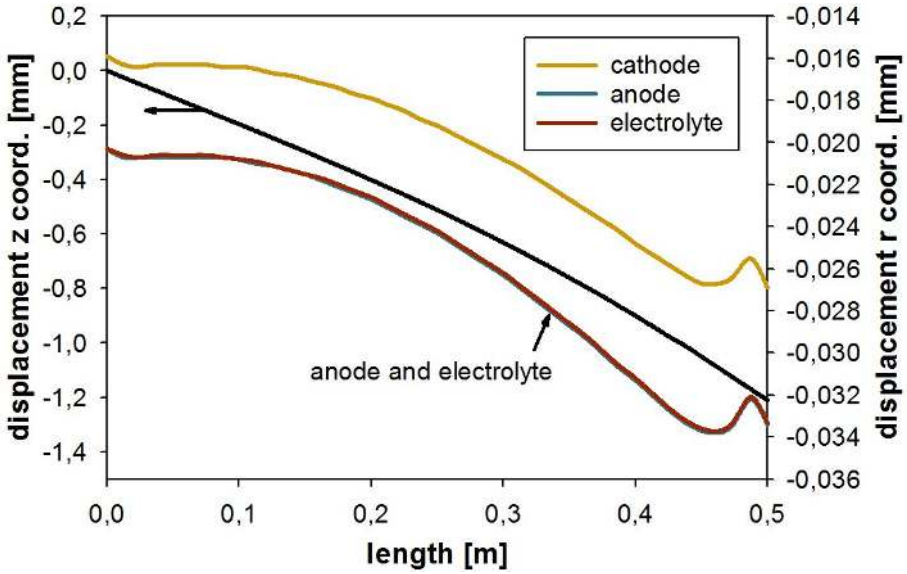

Figure 7: Displacement for electrolyte and electrodes over stack length.

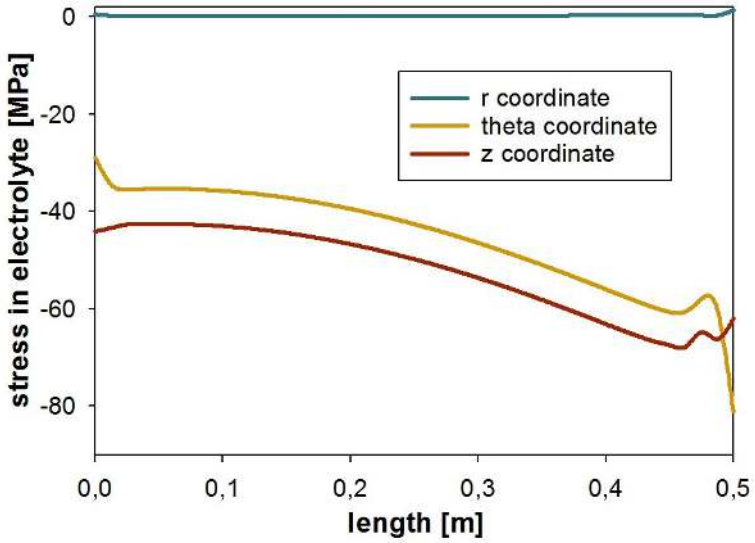

Figure 8: Stress distribution for electrolyte.

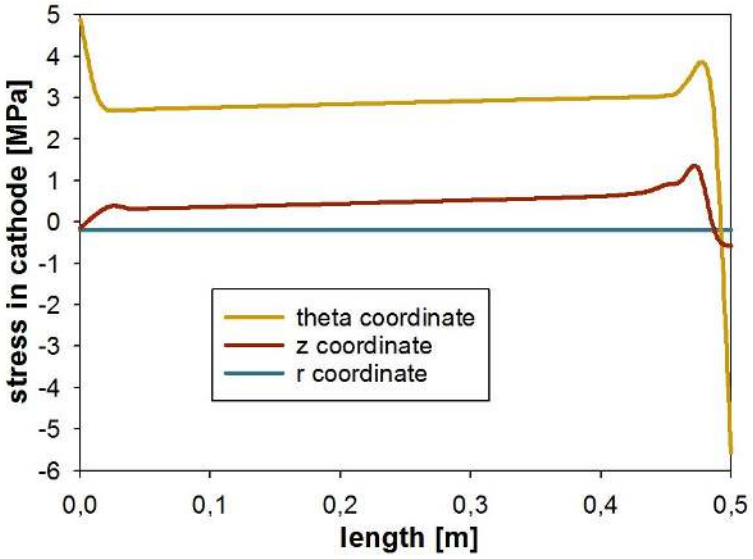

Figure 9: Stress distribution for cathode.

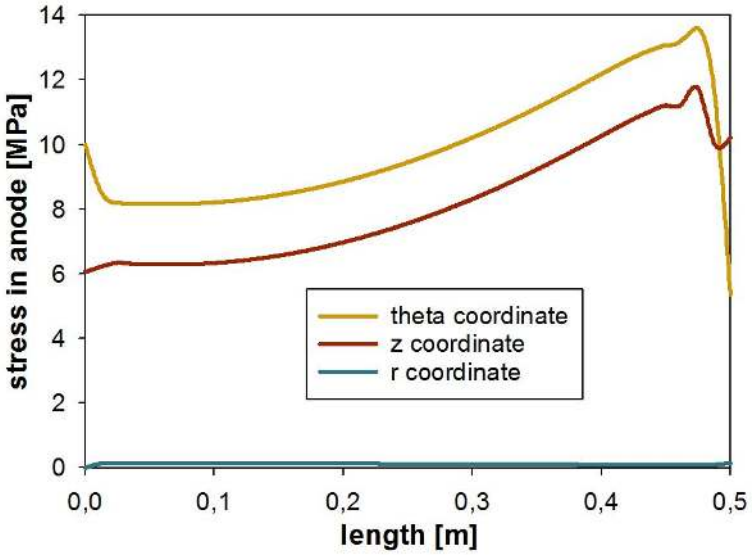

Figure 10: Stress distribution for anode.

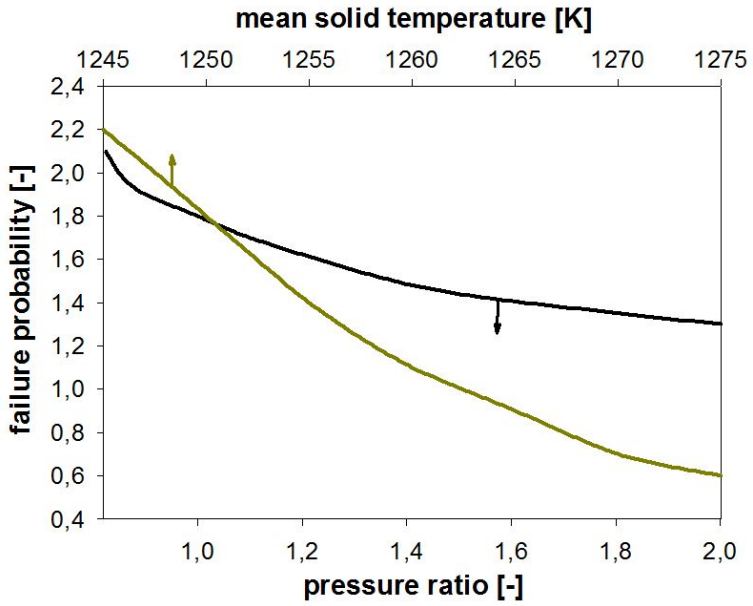

Figure 11: Overall failure probability as function of mean solid temperature and pressure ratio.

Table 3: Default input parameters for simulation.

parameter	**value**
sintering temperature [K]	1473 [34]
stack length [m]	0,5
inlet air temperature [K]	983
inlet air mole flow [mol/s]	15,3
inlet air mole fraction [-]	0,79 N_2, 0,21 O_2
inlet air pressure [kPa]	200
inlet fuel temperature [K]	1310
inlet fuel mole flow [mol/s]	1
inlet fuel mole fraction [-]	1 H_2
inlet fuel pressure [kPa]	200
DC power output [kW]	87
voltage [V]	0,52
current density [A/cm^2], (current [A])	0,5 (139)
fuel utilisation [-]	0,85
mean solid material temperature [K]	1250

Table 4: Comparison of actual operation conditions and specified design and operation constraints.

quantity	**defined (Table 1)**	**simulated**
min. temperature [K]	900	1186
max. temperature [K]	1300	1289
max. current density [kA/m^2]	-	5 (set)
max. temperature gradients (during transients) [K/cm]	20	5
max. temperature difference over length [K]	150	103
fuel utilisation range [-]	0,4-0,9	0,85 (set)
max. pressure difference [bar]	3	$\ll$1
min. air-to-fuel ratio [-]	1	$\gg$1

Table 5: Survival probabilities and overall failure probabilty.

parameter	**simulation result**
P_s^{an} [-]	99,8
P_s^{ca} [-]	99,9
P_s^{el} [-]	98,4
P_f^{system} [-]	1,8

perature (zero stress temperature during manufacturing), will have a detrimental effect on the material's survival probabilities. Off-design operation conditions (also during transients) need therefore be carefully chosen and controlled to keep the system in a safe region.

A potential avenue for further investigation is to incorporate the effect of porosity on thermo-mechanical properties such as the Youngs modulus (see e.g., Ref. [51]).

6 Acknowledgement

Dr Christoph Stiller is gratefully acknowledged for providing the original SOFC model code. We thank the anonymous reviewers for their time to review the paper and their very good comments and recommendations.

References

[1] A. Choudhury, H. Chandra, and A. Arora, "Application of solid oxide fuel cell technology for power generation - a review," *Renewable and Sustainable Energy Reviews*, vol. 20, pp. 430 – 442, 2013.

[2] D. Hickey, M. Alinger, A. Shapiro, K. Brown, T. Striker, H. Wang, S. Gaunt, D. Kinsey, and I. Hussainia, "Stack development at ge-fuel cells," *ECS Trans*, vol. 78, no. 1, pp. 107–116, 2017.

[3] N. Q. Minh, "Ceramic fuel cells," *Journal of the American Ceramic Society*, vol. 76, no. 3, pp. 563–588, 1993.

[4] S. Singhal, "Advances in solid oxide fuel cell technology," *Solid State Ionics*, vol. 135, no. 1, pp. 305 – 313, 2000. Proceedings of the 12th International Conference on Solid State.

[5] A. Stambouli and E. Traversa, "Solid oxide fuel cells (sofcs): a review of an environmentally clean and efficient source of energy," *Renewable and Sustainable Energy Reviews*, vol. 6, no. 5, pp. 433 – 455, 2002.

[6] S. D. Vora, G. Jesionowski, and M. C. Williams, "Overview of u.s. department of energy office of fossil energy's solid oxide fuel cell program for fy2019," *Electrochemical Society Transactions*, vol. 91, pp. 27–39, 2019.

[7] C.-Y. Wang, "Fundamental models for fuel cell engineering," *: Chem. Rev.*, vol. 104, no. 10, pp. 4727–4766, 2004.

[8] O. Yamamoto, "Solid oxide fuel cells: fundamental aspects and prospects," *Electrochimica Acta*, vol. 45, no. 15, pp. 2423 – 2435, 2000.

[9] X. Zhang, S. Chan, G. Li, H. Ho, J. Li, and Z. Feng, "A review of integration strategies for solid oxide fuel cells," *Journal of Power Sources*, vol. 195, no. 3, pp. 685 – 702, 2010.

[10] M. Hubert, J. Laurencin, P. Cloetens, B. Morel, D. Montinaro, and F. Lefebvre-Joud, "Impact of nickel agglomeration on solid oxide cell operated in fuel cell and electrolysis modes," *Journal of Power Sources*, vol. 397, pp. 240 – 251, 2018.

[11] J. Laurencin, M. Hubert, D. F. Sanchez, S. Pylypko, M. Morales, A. Morata, B. Morel, D. Montinaro, F. Lefebvre-Joud, and E. Siebert, "Degradation mechanism of la0.6sr0.4co0.2fe0.8o3-d/gd0.1ce0.9o2-d composite electrode operated under solid oxide electrolysis and fuel cell conditions," *Electrochimica Acta*, vol. 241, pp. 459 – 476, 2017.

[12] N. Q. Minh and M. B. Mogensen, "Reversible solid oxide fuel cell technology for green fuel and power production," *he Electrochemical Society Interface*, 2013.

[13] T. T. Molla, K. Kwok, and H. L. Frandsen, "Modeling the mechanical integrity of generic solid oxide cell stack designs exposed to long-term operation," *Fuel Cells*, vol. 19, no. 1, pp. 96–109, 2019.

[14] A. Nakajo, C. Stiller, G. Harkegard, and O. Bolland, "Modeling of thermal stresses and probability of survival of tubular sofc," *Journal of Power Sources*, vol. 158, no. 1, pp. 287 – 294, 2006.

[15] A. Nakajo, F. Mueller, J. Brouwer, J. V. herle, and D. Favrat, "Mechanical reliability and durability of sofc stacks. part i : Modelling of the effect of operating conditions and design alternatives on the reliability," *International Journal of Hydrogen Energy*, vol. 37, no. 11, pp. 9249 – 9268, 2012.

[16] A. Nakajo, F. Mueller, J. Brouwer, J. V. herle, and D. Favrat, "Mechanical reliability and durability of sofc stacks. part ii: Modelling of mechanical failures during ageing and cycling," *International Journal of Hydrogen Energy*, vol. 37, no. 11, pp. 9269 – 9286, 2012.

[17] M. Navasa, X.-Y. Miao, and H. L. Frandsen, "A fully-homogenized multiphysics model for a reversible solid oxide cell stack," *International Journal of Hydrogen Energy*, vol. 44, no. 41, pp. 23330 – 23347, 2019.

[18] M. Peksen, "3d transient multiphysics modelling of a complete high temperature fuel cell system using coupled cfd and fem," *International Journal of Hydrogen Energy*, vol. 39, no. 10, pp. 5137 – 5147, 2014.

[19] P. Pianko-Oprych, T. Zinko, and Z. Jaworski, "Modeling of thermal stresses in a microtubular solid oxide fuel cell stack," *Journal of Power Sources*, vol. 300, pp. 10 – 23, 2015.

[20] M. F. Serincan, U. Pasaogullari, and N. M. Sammes, "Thermal stresses in an operating micro-tubular solid oxide fuel cell," *Journal of Power Sources*, vol. 195, no. 15, pp. 4905 – 4914, 2010.

[21] M. Peksen, "Numerical thermomechanical modelling of solid oxide fuel cells," *Progress in Energy and Combustion Science*, vol. 48, pp. 1 – 20, 2015.

[22] A. Dubois, K. Taghikhani, J. R. Berger, H. Zhu, R. P. OHayre, R. J. Braun, R. J. Kee, and S. Ricote, "Chemo-thermo-mechanical coupling in protonic ceramic fuel cells from fabrication to operation," *Journal of The Electrochemical Society*, vol. 166, no. 13, pp. F1007–F1015, 2019.

[23] X. Lin, X. Hao, A. Ivanco, Z. Liu, and W. Jia, "Physics-based and control-oriented modeling of diffusion-induced stress in li-ion batteries," *Journal of The Electrochemical Society*, vol. 165, no. 10, pp. A2255–A2266, 2018.

[24] J. Marcicki, M. Zhu, A. Bartlett, X. G. Yang, Y. Chen, T. Miller, P. L'Eplattenier, and I. Caldichoury, "A simulation framework for battery cell impact safety modeling using ls-dyna," *Journal of The Electrochemical Society*, vol. 164, no. 1, pp. A6440–A6448, 2017.

[25] M. Masmoudi, Z. Moumni, and F. Bidault, "Analysis of the thermo-mechanical-chemical coupled response of a lithium-ion battery particle during a charge-discharge cycle," *Journal of The Electrochemical Society*, vol. 166, no. 3, pp. A5445–A5461, 2019.

[26] C. Stiller, *Design, operation and control modelling of SOFC/GT hybrid systems.* PhD thesis, NTNU, 2006.

[27] C. Stiller, B. Thorud, O. Bolland, R. Kandepu, and L. Imsland, "Control strategy for a solid oxide fuel cell and gas turbine hybrid system," *Journal of Power Sources*, vol. 158, no. 1, pp. 303 – 315, 2006.

[28] R. O'Hayre, S. Cha, W. Colella, and F. B. Prinz, *Fuel Cell Fundamentals.* John Wiley & Sons., 2016.

[29] A. L. Dicks and D. A. J. Rand, *Fuel Cell Systems Explained.* John Wiley & Sons Ltd., 2018.

[30] J. W. Fergus, *Solid Oxide Fuel Cells*, ch. 14, pp. 671–700. John Wiley & Sons, Ltd, 2012.

[31] P. J. Gellings and H. J. Bouwmeester, *Handbook of Solid State Electrochemistry.* CRC, 1997.

[32] P.-W. Li and M. K. Chyu, "Simulation of the chemical/electrochemical reactions and heat/mass transfer for a tubular sofc in a stack," *Journal of Power Sources*, vol. 124, no. 2, pp. 487 – 498, 2003.

[33] "Process systems enterprise. the advanced process modelling company."

[34] N. Hildenbrand, B. A. Boukamp, P. Nammensma, and D. H. Blank, "Improved cathode/electrolyte interface of sofc," *Solid State Ionics*, vol. 192, no. 1, pp. 12 – 15, 2011.

[35] R. B. Hetnarski and M. R. Eslami, *Thermal Stresses-Advanced Theory and Applications*. Springer, 2019.

[36] M. Sadd, "Elasticity," p. iii, Boston: Academic Press, third edition ed., 2009.

[37] S. Timoshenko and J. N. Goodier, *Theory of Elasticity*. Mcgraw Hill Education, 1970.

[38] J. Kelly, "Perspectives on strength," *Dental Materials*, vol. 11, no. 2, pp. 103 – 110, 1995.

[39] S. Suresh, *Fatigue of Materials*. Cambridge University Press, 1998.

[40] R. B. Bird, W. E. Stewart, and E. N. Lightfoot, *Transport Phenomena*. Wiley, 2006.

[41] G. Allaire, *Numerical analysis and optimization. An introduction to mathematical modelling and numerical simulation*. Oxford University Press, 2007.

[42] F. Greco, H. Frandsen, A. Nakajo, M. F. Madsen, and J. V. herle, "Modelling the impact of creep on the probability of failure of a solid oxide fuel cell stack," *Journal of the European Ceramic Society*, vol. 34, no. 11, pp. 2695 – 2704, 2014. Modelling and Simulation meet Innovation in Ceramics Technology.

[43] S. Giraud and J. Canel, "Young's modulus of some sofcs materials as a function of temperature," *Journal of the European Ceramic Society*, vol. 28, no. 1, pp. 77 – 83, 2008.

[44] A. Selçuk, G. Merere, and A. Atkinson, "The influence of electrodes on the strength of planar zirconia solid oxide fuel cells," *Journal of Materials Science*, vol. 36, pp. 1173–1182, Mar 2001.

[45] G. Anandakumar, N. Li, A. Verma, P. Singh, and J.-H. Kim, "Thermal stress and probability of failure analyses of functionally graded solid oxide fuel cells," *Journal of Power Sources*, vol. 195, no. 19, pp. 6659 – 6670, 2010.

[46] J. H. Won Yong Lee and A. F. Ghoniem, "On the predictions of carbon deposition on the nickel anode of a sofc and its impact on open-circuit conditions," *Journal of The Electrochemical Society*, vol. 160, no. 2, pp. F94–F105, 2013.

[47] V. Subotic, C. Schluckner, B. Stockl, V. Lawlor, H. Schroettner, and C. Hochenauer, "Strategy for carbon gasification from porous ni-ysz anodes of industrial-sized asc-sofcs and effects of carbon growth," *Journal of The Electrochemical Society*, vol. 163, no. 14, pp. F1515–F1522, 2016.

[48] H. Sumi, Y.-H. Lee, H. Muroyama, T. Matsui, M. Kamijo, S. Mimuro, M. Yamanaka, Y. Nakajima, and K. Eguchi, "Effect of carbon deposition by carbon monoxide disproportionation on electrochemical characteristics at low temperature operation for solid oxide fuel cells," *Journal of Power Sources*, vol. 196, no. 10, pp. 4451 – 4457, 2011.

[49] N. Mahato, A. Banerjee, A. Gupta, S. Omar, and K. Balani, "Progress in material selection for solid oxide fuel cell technology: A review," *Progress in Materials Science*, vol. 72, pp. 141 – 337, 2015.

[50] S. Zha, Z. Cheng, and M. Liu, "Sulfur poisoning and regeneration of ni-based anodes in solid oxide fuel cells," *Journal of The Electrochemical Society*, vol. 154, no. 2, pp. B201–B206, 2007.

[51] M. Pihlatie, A. Kaiser, and M. Mogensen, "Mechanical properties of nio/ni-ysz composites depending on temperature, porosity and redox cycling," *Journal of the European Ceramic Society*, vol. 29, no. 9, pp. 1657 – 1664, 2009.